Vacuum 222 (2024) 112961

Contents lists available at ScienceDirect

Vacuum

journal homepage: www.elsevier.com/locate/vacuum

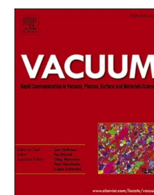

Improvement of the resistivity uniformity of 8-inch 4H–SiC wafers by optimizing the thermal field

Guojie Hu [a], Guanglei Zhong [a], Xixi Xiong [a], Huadong Li [a], Hongyu Shao [a], Laibin Zhao [a], Xiaomeng Li [a,*], Xianglong Yang [a,**], Xiufang Chen [a], Xuejian Xie [a], Yan Peng [a], Guojian Yu [b], Xiaobo Hu [a], Xiangang Xu [a]

[a] .State Key Laboratory of Crystal Materials, Institute of Novel Semiconductors, Shandong University, Jinan, 250100, People's Republic of China
[b] .Guangzhou Summit Crystal Semiconductor Co., Ltd, Guangzhou, 511462, People's Republic of China

ARTICLE INFO

Handling Editor: Prof. L.G. Hultman

Keywords:
8-inch,4H–SiC
Resistivity uniformity
Thermal field
PVT

ABSTRACT

8-inch *N*-type 4H–SiC single crystals were grown on 4° off-axis seeds by the physical vapor transport (PVT) method. The electrical properties of 8-inch 4H–SiC wafers were assessed by contactless resistivity mapping. The resistivity of the whole wafer is inhomogeneous with an inhomogeneity of 4.8 %, much higher than that of standard 6-inch wafers with a resistivity inhomogeneity of 1.2 %. This nonuniformity phenomenon is attributed to facet formation caused by discontinuities in the thermal field as the crystal diameter increases. Due to the facet effect, the nitrogen doping concentration in the facet region is higher than that in other regions. By optimizing the thermal field through adjustment of the growth conditions, a nearly flat and slightly convex 8-inch SiC crystal growth interface was obtained. The uniformity of the resistivity of 8-inch SiC wafers is significantly improved, with an inhomogeneity of 1.6 %.

1. Introduction

Silicon carbide (SiC) crystals have exceptional physical and electrical properties, including a wide band gap, a high critical breakdown electric field, a high thermal conductivity, a high carrier saturation velocity, and excellent chemical stability, and are therefore widely used under severe conditions [1–4]. The demand for SiC devices in automotive applications is increasing due to the accelerated popularization of new energy vehicles and the widespread use of 800 V high-voltage fast-charging platforms [5]. Currently, 6-inch commercial SiC substrates dominate the market [6,7]. However, the SiC substrate cost is still high, but increasing the SiC crystal diameter and improving the crystal quality is an efficient approach to reducing the device cost, making 8-inch SiC wafers a promising mainstream choice for industrial production [5].

However, as the crystal diameter increases from 150 mm to 200 mm, the difficulty of controlling multiple physical fields significantly multiplies, especially with respect to the thermal field, which plays a critical role in the growth process of large SiC crystals. Due to the larger size of the growth crucible, the thermal resistance increases from the outside to the inside. Consequently, the temperature at the center of the crystal and the raw material decreases, while the radial temperature gradient increases, resulting in irregular crystal shapes. Due to the relatively high temperature at the edges of the raw materials, the decomposition rate is higher than that at the center, leading to vigorous gas flow near the crucible walls. Consequently, the growth rate at the outer edges of the crystals is accelerated. During crystal growth, the formation of "M"-shaped crystals is influenced by the surrounding polycrystalline structure [8]. This, consequently, leads to an increase in microdefects, including polytypes [9], cracks, micropipes, and dislocations [10,11], during the growth of 8-inch SiC crystals.

Substrate resistivity uniformity is a critical issue for 4H–SiC substrates used for power devices. Substrate resistivity inhomogeneity causes a variation in the on-resistance of vertical SiC power devices when 4H–SiC substrates with such inhomogeneity are used for device fabrication. The inhomogeneity of the substrate resistivity caused by the inhomogeneity of the nitrogen doping concentration could also lead to a greater misfit between the substrate and the homoepitaxial layer grown on it, resulting in the introduction of misfit dislocations in the epilayer. So a conductive substrate that has a uniform radial distribution of resistivity across its surface must be obtained to ensure the high

* Corresponding author.
** Corresponding author.
E-mail addresses: lixiaomeng@sdu.edu.cn (X. Li), yangxl2016@sdu.edu.cn (X. Yang).

https://doi.org/10.1016/j.vacuum.2024.112961
Received 20 October 2023; Received in revised form 19 December 2023; Accepted 4 January 2024
Available online 10 January 2024
0042-207X/© 2024 Elsevier Ltd. All rights reserved.

performance of power devices. Notably, the resistivity of 8-inch conductive SiC is affected by the temperature during the growth process. At higher temperatures, the nitrogen doping is reduced, causing the resistance of SiC to increase. The radial temperature gradient across the crystal growth surface causes lower nitrogen doping and higher resistivity at the edges of the crystal than at the center [12]. As the diameter of the crystal increases, the temperature gradient in the radial direction increases. This makes the problem of uneven nitrogen doping and resistivity even more apparent. Consequently, the achievement of uniform resistivity in 8-inch *N*-type SiCis a significant challenge that needs to be addressed.

To successfully overcome the challenges of growing 8-inch *N*-type SiC crystals, the physical environment, especially the thermal field, must be precisely controlled. Furthermore, the crystal growth crucible must be carefully designed and optimized and the appropriate growth process parameters established to obtain high-quality crystals. PVT is a semi-closed black-box growth technique that prohibits direct observation of process parameters under high temperature conditions from an experimental perspective. Numerical simulation can rapidly provide dependable results and significantly decrease the cost of experimentation [8, 13–15]. Such efforts will enhance the quality and usability of these crystals, making the application of SiC devices in various sectors, especially the development of electric vehicles, easier.

This study focuses on the problem of resistivity nonuniformity in 8-inch *N*-type SiC crystals and discusses the origin and formation mechanisms of two facets. With the help of VR-PVT software simulation, we optimize the thermal field by modifying the mounting conditions. This leads to an improvement in the crystal surface morphology, resulting in a nearly flat microconvex crystal, which enhances the resistivity uniformity. Subsequently, the crystal is cut, ground, and polished to obtain SiC wafers with improved resistivity uniformity. These findings are anticipated to boost the implementation of SiC devices in various fields, including new energy vehicles.

2. Experiment

The growth of 8-inch *N*-type 4H–SiC single crystals was carried out by the sublimation method within a temperature range of 2000–2400 °C. The growth process was performed on a 4° off-axis 4H–SiC seed in a graphite crucible, and the growth direction was approximately parallel to the c-axis. Induction coils were used to heat the crucible, with SiC powder placed at the bottom of the crucible as the source material. The growth pressure was maintained at 1–5 mbar, and argon gas was used as the carrier gas. Temperature measurements were performed at the top lid via color pyrometry. During the growth process, nitrogen was introduced as a donor dopant by flowing N_2 gas. After short-term growth for 50 h, the macroscopic surface morphology of the 4H–SiC crystal was observed using an optical microscope. In addition, the 4H–SiC single crystal was processed into standard 8-inch SiC substrates. The resistivity of the wafers was tested using contactless

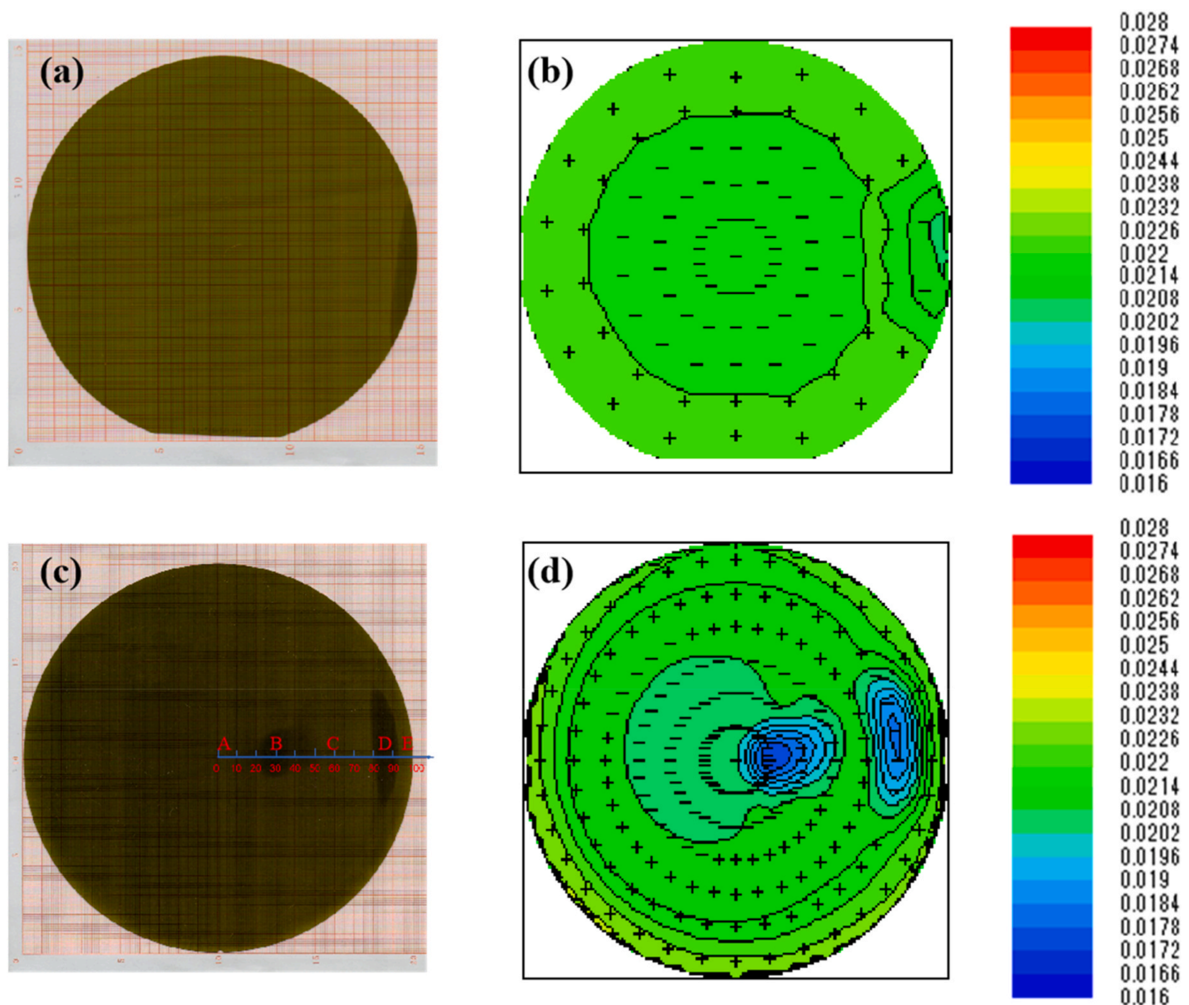

Fig. 1. Image of a polished wafer and its resistivity before optimization:(a) Image of a polished standard 6-inch *N*-type SiC wafer; (b) resistivity of a polished standard 6-inch *N*-type SiC wafer; (c) image of a polished 8-inch *N*-type SiC wafer before optimization; (d) resistivity of a polished standard 8-inch *N*-type SiC wafer before optimization.

resistivity measurements. The wafers were subjected to contactless resistivity measurement. Raman scattering spectra of n-type 4H–SiC substrates were obtained in a backscattering configuration by using a Horiba Jobin Yvon HR 800 system at room temperature. An excitation source of a 532 nm laser (40 mW) was used as the excitation source. A resolution of 0.1 cm^{-1} was used for the Raman spectroscopy.

3. Results and discussion

6-and 8-inch crystals were grown in a mixed gas with the same proportion of doped nitrogen gas. Fig. 1(a) displays a standard 6-inch *N*-type SiC wafer with a dark surface area at the edge. Fig. 1(b) illustrates a high degree of resistivity uniformity across the wafer. The minimum resistivity value recorded is 0.0209 Ω-cm, the maximum value is 0.0225 Ω-cm, and the average resistivity is 0.2199 Ω-cm, meeting the industry requirements of 0.015–0.025Ω-cm. At the same time, the resistivity inhomogeneity of the 6-inch *N*-type SiC wafer is only 1.21 %, showing good distribution uniformity. The uniformity of the resistivity of the 8-inch crystal has significantly decreased, although it grew in a mixed gas with the same nitrogen doping ratio as the 6-inch crystal. Fig. 1(c) presents two dark-side regions on an 8-inch *N*-type SiC wafer. Furthermore, Fig. 1(d) demonstrates the low resistivity of the two dark-side areas. As the SiC wafer grows in size, it becomes color-inhomogeneous, indicating a worse resistivity inhomogeneity. Thiele's theory [16,17] suggests that selective interfacial adsorption causes the formation of specific facets in crystals at a macroscopic scale. The adsorption effect decreases the surface free energy of the crystals, resulting in an increased nitrogen concentration and a darker color in certain small surface regions relative to other regions. The small dark surface regions have higher nitrogen doping concentrations that lead to reduced resistivity. This produces poor resistivity uniformity across the wafer. The 8-inch *N*-type SiC wafer resistivity ranges from 0.01740 to 0.02289 Ω-cm along the radial direction, and the average resistivity of 8-inch wafers is 0.2088Ω-cm, about 5 % lower than 6-inch wafers, meeting the industry requirements of 0.015–0.025Ω-cm as well. Meanwhile, the resistivity inhomogeneity of the 8-inch *N*-type SiC wafer is 4.82 %, as displayed in Fig. 1(d). Raman spectroscopy was used to evaluate different regions of Fig. 1(c). Fig. 2 shows that regions B and D have a relatively high concentration of nitrogen. In these areas, the LOPC mode shifts to higher wavelengths, the peak intensity decreases, and the full-width at half-maximum (FWHM) gradually widens. This occurrence is consistent with prior research [18]. The phenomenon is caused by the coupling of the longitudinal optical phonon FLO mode with the plasma constituent, which results in the formation of the LOPC mode. The frequency of both the high-frequency branch (L+) and the low-frequency branch (L-) changes as the carrier concentration varies after coupling. This feature is a useful tool for calculating the carrier concentration. Due to overdamping, only (L+) modes are observed for SiC. S. Nakashima et al. [19] demonstrated a linear relationship between the doping concentration in 4H–SiC and the frequency shift of the LOPC mode:

$$n \approx \frac{\varepsilon_\infty m^*}{4\pi e^2} \frac{2\omega_{LO}}{(1-\varepsilon_\infty/\varepsilon_0)} \Delta\omega \quad (1)$$

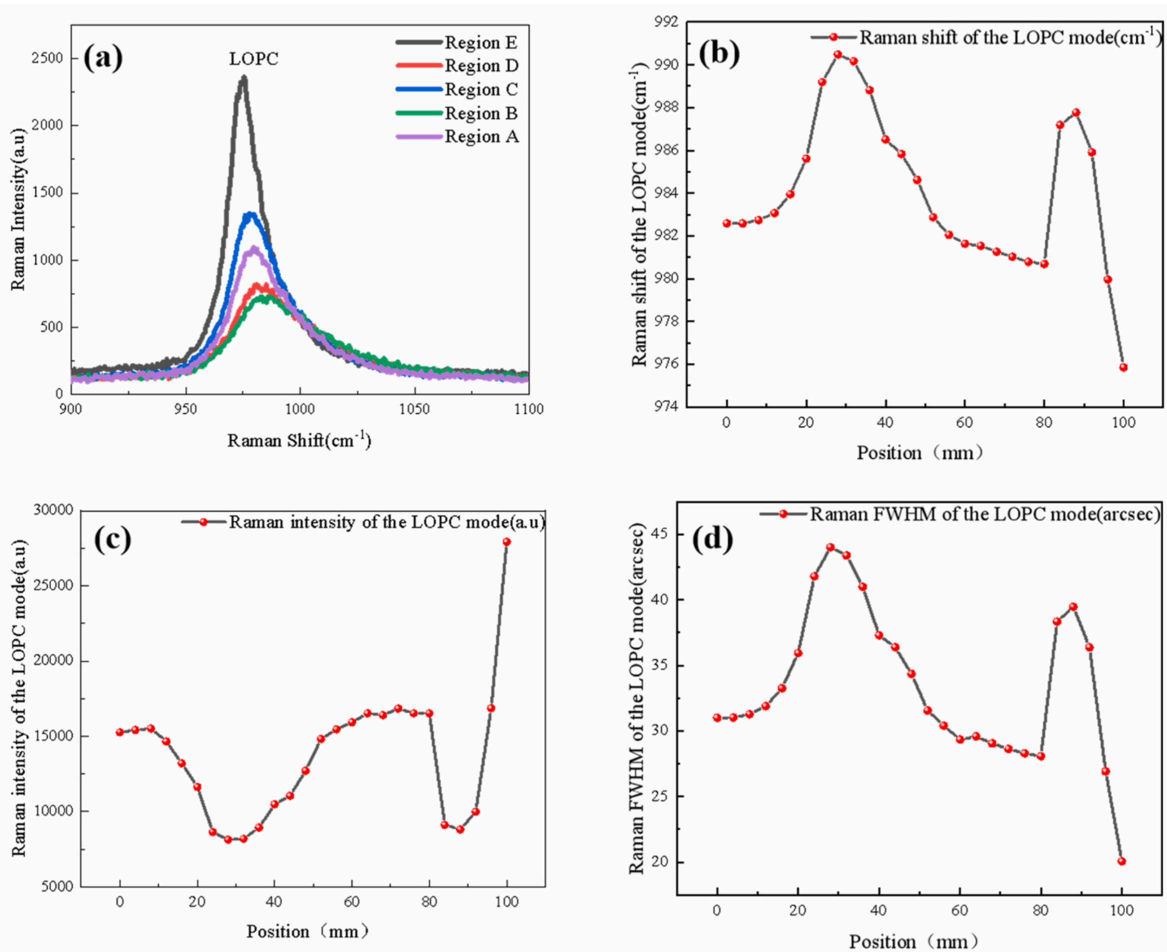

Fig. 2. (a) Raman spectra of different regions of the wafer before optimization; (b)Variation of Raman shift of the LOPC mode with position; (c) Variation of Raman intensity of the LOPC mode with position; (d) Variation of Raman FWHM of the LOPC mode with position.

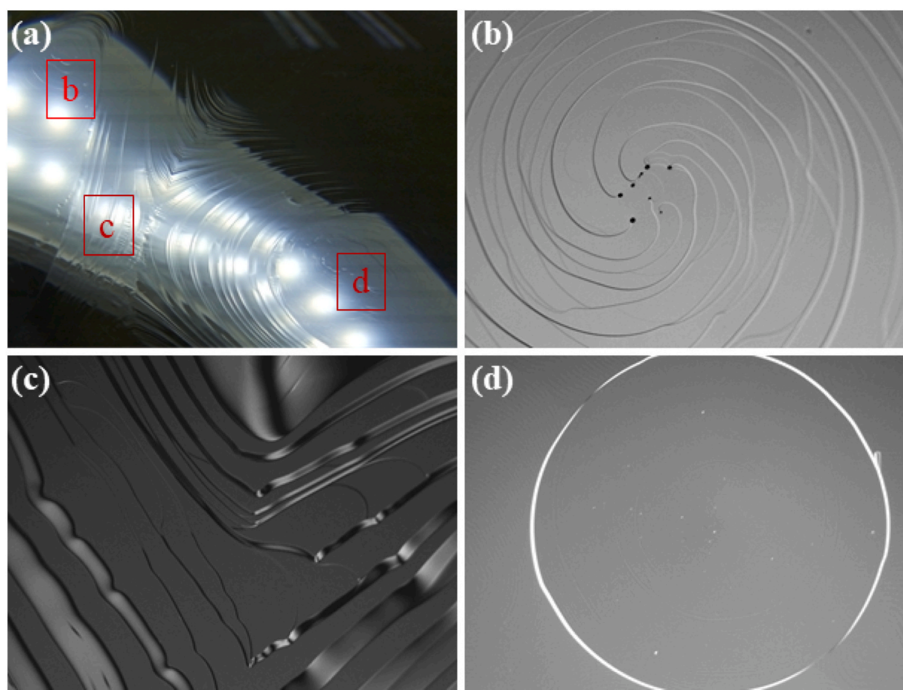

Fig. 3. (a) There are two facets on the crystal surface; (b) there are circular steps in the facet area; (c) the step flows of the two small faces collide; (c) the facet exhibits concentric circles.

Where n is the doping concentration in 4H–SiC, ε and ε_∞ represent the dielectric constants at static and high frequencies, respectively. Moreover, m^* is the 4H–SiC effective mass, and Δω is the frequency shift of the LOPC mode concerning the frequency of the undoped sample ω_{LO}.

In the case of 4H–SiC, the effective mass $m^* = 0.29m_0$ resulting in a linear relationship between Δω and as [19]:

$$n = 1.23 \times 10^{17} \Delta\omega \quad (2)$$

Therefore, in high resistivity and high nitrogen doped regions, the LOPC mode shifts to higher wavelengths. The thermal field in crystal growth affects the amount of nitrogen doping and the resistivity of the crystal. To study the phenomenon of uneven resistivity of 8-inch wafers, the thermal field situation of the 8-inch SiC crystal is discussed.

To study the thermal field situation of the 8-inch SiC crystal, short-term growth of crystals was performed for 50 h. As shown in Fig. 3(a), optical microscopy revealed that the crystals grown before optimization of the thermal field had two distinct facet regions. In region (b), a circular spiral step flow is observed on the $(000\ \overline{1})$ surface, whereas in region (d), a concentric circular step flow is observed on the $(000\ \overline{1})$ surface. These two step flows intersect in region (c). In region (b), the formation of spiral steps is caused by the growth mechanism of screw dislocations on the crystal surface. Due to the exposed screw dislocation heads on the crystal surface, these spiral steps do not disappear during the growth process. In fact, the spiral steps converge and split under the influence of impurity adsorption, defect blocking and other factors, resulting in step bunching at the edges of the small-face region. These phenomena break the original sixfold symmetry of the crystal, resulting in a circular shape. The hillock-shaped small face shown in region (d) is composed of concentric circular steps. This occurs because the distance between a pair of left and right screw dislocations exceeds the critical nucleus diameter, which triggers the development of a closed step flow (see Fig. 3).

When 4H–SiC is grown on a 4° off-axis seed, the symmetry axis of the thermal field forms a 4° angle with $<000\ \overline{1}>$. When the orientation of the local growth interface significantly deviates from the singular plane $(000\ \overline{1})$, the step density at the interface is high, and the step width is less than the diffusion length of the surface adsorbed atoms. In this case, the diffusion of surface atoms does not affect the growth rate, leading to step flow growth. When the orientation of the locally grown interface is very close to the singular plane $(000\ \overline{1})$, the step density is low, and the step width is much larger than the diffusion length of the surface adsorbed atoms. In this case, the diffusive motion of the surface-adsorbed Si and C atoms becomes the main limiting factor for the growth rate in this region, leading to a slowdown in the growth rate and the formation of a facet. There are dislocation outcrop points in the facet, and under certain supersaturation, the conditions required for spiral dislocation growth are satisfied. The growth mode is spiral dislocation growth mode, that is, the dislocation outcrop points on the interface form spiral steps to promote growth, as shown in Fig. 4.

The assembly structure is shown in Fig. 5(a). The thermal field of the 8-inch SiC crystal under the above mounting conditions was simulated using VR-PVT software, and the simulation result of the temperature field distribution in the growth cell is shown in Fig. 5(b), and the temperature field of the 8 inch SiC crystal is shown in Fig. 5(c). The temperature field distribution of this growth cell is uneven, and the temperature field is not continuous in the crystal growth surface area, resulting in an uneven and undulating crystal surface shape, forming two convex surface small areas on the crystal.

The two facet regions on the SiC crystal surface are closely related to the shape of the 8-inch SiC crystal growth front. Typically, the shape of

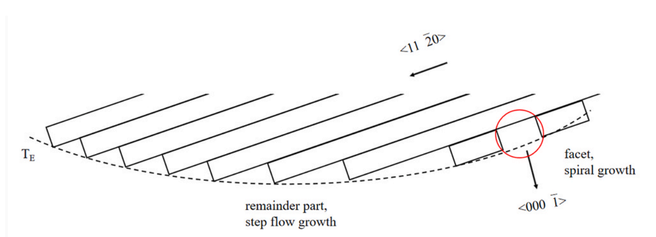

Fig. 4. Schematic diagram of growth mechanism of SiC single crystal using 4° off-axis 4H–SiC $\{000\ \overline{1}\}$ face seed.

Fig. 5. (a) Assembly structure before the optimization; (b)the temperature field distribution in the growth cell before optimization; (c) the temperature field of the 8 inch SiC crystal before optimization.

the SiC crystal growth front is believed to be determined by the thermal field, following isothermal lines [12,17]. With the increase in seed diameter to 8 inch, the continuity of the thermal field decreases, and the equilibrium isothermal line T_E is shown in Fig. 6. The crystal surface with an orientation of approximately <000 $\overline{1}$> is exposed to the vapor. At this point, the step density on the surface is low, and the adsorption of Si and C atoms on the surface limits the crystal growth rate, resulting in a slow growth rate in this region. Through this process, two small facet regions with a <000 $\overline{1}$ > orientation are formed. Dislocation outcrops exist in the two facet regions and under certain supersaturations the conditions required for spiral dislocation growth exist. The growth mode is spiral dislocation growth mode. This means that the dislocation outcrops at the interface form spiral steps to promote growth.

Before optimization, the temperature field of the 8-inch crystal growth rises and falls, and the surface of the growing crystal fluctuates. To correct this phenomenon, we used VR-PVT software to optimize the thermal field under the above assembly conditions. The mountain-shaped shelter structure was placed on the crucible lid as shown in Fig. 7(a). This shelter structure can effectively regulate the temperature field and the gas flow near the crucible wall. The temperature field simulation of the optimized assembly showed that the temperature field distribution within the growth cell is more uniform in the shelter structure as shown in Fig. 7(b). The temperature field distribution of the crystal is relatively flat, and the 8-inch crystal shape is almost flat and slightly convex as shown in Fig. 7(c).

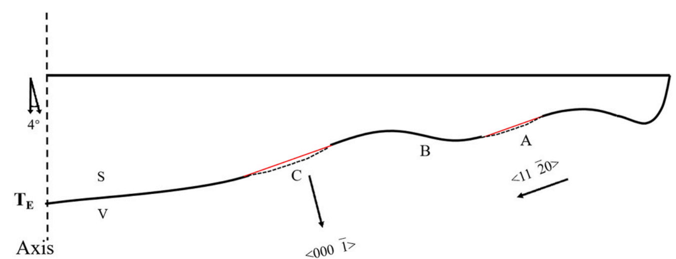

Fig. 6. Schematic diagram of facets forming at the crystal interface.

With the help of the simulation results of the thermal field obtained by VR-PVT software, the assembly structure was optimized, and an 8-inch SiC single crystal with an almost flat microconvex surface and only a small facet was successfully grown. Notably, the almost flat microconvex surface reduces the step height of the nonsurface regions, thereby reducing the incorporation of impurities into these regions, leading to an increase in the carrier concentration and improving the

Fig. 7. (a) Assembly structure after the optimization; (b) the temperature field distribution in the growth cell after optimization; (c) the temperature field of the 8 inch SiC crystal after optimization.

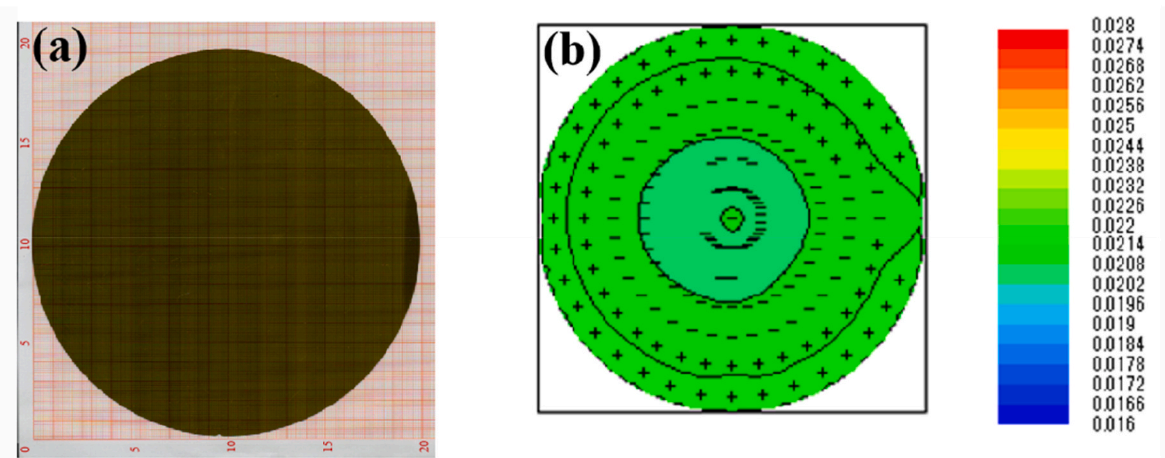

Fig. 8. Image of a polished wafer and its resistivity after optimization (a) image of a polished 8-inch *N*-type SiC wafer after optimization; (b) resistivity of a polished standard 8-inch *N*-type SiC wafer after optimization.

resistivity uniformity of the crystal [18]. After being cut, ground, and polished, the crystals were transformed into 8-inch SiC wafers and tested for resistivity. The test results indicate that the wafers have a small facet at the edge, as shown in Fig. 8(a), and the color is uniform throughout. The resistivity uniformity within the wafer, as shown in Fig. 8(b), is good, with a maximum resistivity of 0.02187 Ω-cm and a minimum resistivity of 0.02069 Ω-cm recorded. The change in resistivity is only 1.61 %, indicating a more uniform distribution and meeting the industry requirement of 0.015–0.025 Ω-cm. These results indicate that the resistivity does not vary significantly in different regions of the crystal, showing good overall resistivity uniformity.

4. Conclusion

In this study, as the crystal size increased, the uniformity of the thermal field sharply decreased, resulting in two facet regions on the 8-inch crystal surface and an increase in the non-uniformity of the 8-inch chip resistivity. This study also confirmed through Raman testing that as the resistivity increases, the peak position of the LOPC mode shifts to higher wavelengths, the peak intensity decreases and the FWHM widens. Temperature-field optimization simulation of eight-inch silicon carbide crystal using VR-PVT software, and a special shelter structure obtained the thermal field with small radial temperature gradient and good distribution uniformity. Based on this temperature field, a nearly flat microconvex 8-inch silicon carbide crystal was obtained. After processing the crystal into an 8-inch SiC wafer, the resistivity uniformity increased significantly, and the resistivity inhomogeneity was only 1.61 %. This provides a simple and feasible way to improve the resistivity uniformity of the 8-inch SiC single crystals grown by the PVT method.

CRediT authorship contribution statement

Guojie Hu: Writing – review & editing, Writing – original draft, Software, Data curation, Conceptualization. **Guanglei Zhong:** Validation. **Xixi Xiong:** Validation. **Huadong Li:** Validation. **Hongyu Shao:** Validation. **Laibin Zhao:** Validation. **Xiaomeng Li:** Validation. **Xianglong Yang:** Writing – review & editing, Data curation, Conceptualization, Supervision. **Xiufang Chen:** Data curation, Conceptualization, Supervision. **Xuejian Xie:** Validation, Conceptualization. **Yan Peng:** Validation. **Guojian Yu:** Validation, Conceptualization. **Xiaobo Hu:** Conceptualization, Supervision. **Xiangang Xu:** Supervision, Resources.

Declaration of competing interest

The authors declare that they have no known competing financial interests or personal relationships that could have appeared to influence the work reported in this paper.

Data availability

Data will be made available on request.

Acknowledgments

This work was financially supported by the National Natural Science Foundation of China (52022052, 62004118), Shandong Province Key R&D Program (2022ZLGX02), Taishan Scholars Program.

References

[1] X. She, A.Q. Huang, O. Lucia, B. Ozpineci, Review of silicon carbide power devices and their applications, IEEE Trans. Ind. Electron. 64 (10) (2017) 8193–8205.
[2] T. Kimoto, Bulk and epitaxial growth of silicon carbide, Prog. Cryst. Growth Char. Mater. 62 (2) (2016) 329–351.
[3] T. Kimoto, Material science and device physics in SiC technology for high-voltage power devices, Jpn. J. Appl. Phys. 54 (4) (2015) 040103.
[4] P.J. Wellmann, Review of SiC crystal growth technology, Semicond. Sci. Technol. 33 (10) (2018) 103001.
[5] M. Musolino, X. Xu, H. Wang, V. Rengarajan, I. Zwieback, G. Ruland, D. Crippa, M. Mauceri, M. Calabretta, A. Messina, Paving the way toward the world's first 200mm SiC pilot line, Mater. Sci. Semicond. Process. 135 (2021) 106088.
[6] Y. Makarov, D. Litvin, A. Vasiliev, S. Nagalyuk, Sublimation Growth of 4 and 6 Inch 4H-SiC Low Defect Bulk Crystals in Ta (TaC) Crucibles, Mater. Sci. Forum, 2016, pp. 101–104.
[7] J.W. Choi, J.G. Kim, B.K. Jang, S.K. Ko, M.O. Kyun, J.D. Seo, K.R. Ku, J.M. Choi, W. J. Lee, Modified Hot-Zone design for large diameter 4H-SIC single crystal growth, Mater. Sci. Forum (2019) 18–21.
[8] S. Zhang, G. Fan, T. Li, L. Zhao, Optimization of thermal field of 150 mm SiC crystal growth by PVT method, RSC Adv. 12 (31) (2022) 19936–19945.
[9] T. Shiramomo, B. Gao, F. Mercier, S. Nishizawa, S. Nakano, Y. Kangawa, K. Kakimoto, Thermodynamical analysis of polytype stability during PVT growth of SiC using 2D nucleation theory, J. Cryst. Growth 352 (1) (2012) 177–180.
[10] T. Nakano, N. Shinagawa, M. Yabu, N. Ohtani, Formation and multiplication of basal plane dislocations during physical vapor transport growth of 4H-SiC crystals, J. Cryst. Growth 516 (2019) 51–56.
[11] B. Gao, K. Kakimoto, Optimization of power control in the reduction of basal plane dislocations during PVT growth of 4H-SiC single crystals, J. Cryst. Growth 392 (2014) 92–97.
[12] D.M. Hansen, G.Y. Chung, M.J. Loboda, A Study of Nitrogen Incorporation in PVT Growth of N+ 4H SiC, Mater. Sci. Forum, 2006, pp. 59–62.
[13] X. Liu, B.-y. Chen, L.-X. Song, E.-W. Shi, Z.-Z. Chen, The behavior of powder sublimation in the long-term PVT growth of SiC crystals, J. Cryst. Growth 312 (9) (2010) 1486–1490.
[14] X. Wang, D. Cai, H. Zhang, A novel method to increase the growth rate in sublimation crystal growth of advanced materials, Int. J. Heat Mass Tran. 50 (7–8) (2007) 1221–1230.
[15] Q.-S. Chen, H. Zhang, R.-H. Ma, V. Prasad, C. Balkas, N. Yushin, Modeling of transport processes and kinetics of silicon carbide bulk growth, J. Cryst. Growth 225 (2–4) (2001) 299–306.
[16] X.L. Yang, K. Yang, X.F. Chen, Y. Peng, X.B. Hu, X.G. Xu, Physical Vapor Transport Growth of 4H-SiC on {000-1} Vicinal Surfaces, Mater. Sci. Forum, 2015, pp. 68–72.
[17] M. Bogdanov, A. Galyukov, S.Y. Karpov, A. Kulik, S. Kochuguev, D.K. Ofengeim, A. Tsiryulnikov, M. Ramm, A. Zhmakin, Y.N. Makarov, Virtual reactor as a new tool for modeling and optimization of SiC bulk crystal growth, J. Cryst. Growth 225 (2–4) (2001) 307–311.
[18] X. Hu, Y. Peng, R. Wei, X. Chen, X. Xu, Characterization of electrical properties of n-type 4H-SiC single crystals by Raman spectroscopy, ECS J. Solid State Sci. Technol. 2 (8) (2013) N3022.
[19] K. Yokomoto, K. Shioura, M. Yabu, M. Nakano, N. Ohtani, Novel characterization method for the nitrogen doping concentration in heavily nitrogen-doped 4H-SiC crystals by Raman scattering microscopy, Jpn. J. Appl. Phys. 59 (5) (2020) 051003.